



UNIVERSITÀ DI PARMA

ARCHIVIO DELLA RICERCA

University of Parma Research Repository

Synthesis, crystal structure, structural phase transition and dielectric properties of new organic-inorganic hybrid compound: $(C_6H_5CH_2N(C_2H_5)_3)CdCl_3$

This is the peer reviewed version of the following article:

Original

Synthesis, crystal structure, structural phase transition and dielectric properties of new organic-inorganic hybrid compound: $(C_6H_5CH_2N(C_2H_5)_3)CdCl_3$ / Dadi, A.; Mazzeo, P. P.; Bacchi, A.; Loukil, M.. - In: JOURNAL OF MOLECULAR STRUCTURE. - ISSN 0022-2860. - 1258:(2022), p. 132617.132617. [10.1016/j.molstruc.2022.132617]

Availability:

This version is available at: 11381/2920249 since: 2022-03-29T17:29:44Z

Publisher:

Elsevier B.V.

Published

DOI:10.1016/j.molstruc.2022.132617

Terms of use:

openAccess

Anyone can freely access the full text of works made available as "Open Access". Works made available

Publisher copyright

(Article begins on next page)

Synthesis, crystal structure, structural phase transition and dielectric properties of new organic-inorganic hybrid compound: $(C_6H_5CH_2N(C_2H_5)_3)CdCl_3$

Ahlem Dadi ^{a,*}, Paolo Pio Mazzeo ^b, Alessia Bacchi ^b, Mohamed Loukil ^a

^a Laboratory of Material Sciences and Environment, Faculty of science of Sfax, University of Sfax, Tunisia

^bUniversity of Parma, Department of Chemistry, Life Sciences and Environmental Sustainability, Parco Area delle Scienze 17/A, 43124 Parma, Italy

Corresponding author: ahlamdadi92@yahoo.com

Abstract

Single crystal of new organic-inorganic hybrid compound, $(C_6H_5CH_2N(C_2H_5)_3)CdCl_3$, was successfully synthesis by slow evaporation method at room temperature and characterized by divers techniques such as single X-ray diffraction, Infrared and Raman spectroscopy, Thermal analysis (TGA and DSC), Variable temperature X-ray powder diffraction (VT-XRPD) and dielectric properties. The results of single X-ray studies demonstrated that the title compound crystallizes in the monoclinic system with the space group $P2_1/n$. The atomic arrangement of the crystal structure can be described as 1D polymeric inorganic chain $CdCl_5$ along the a-axis between which the organic groups are located. It consists on isolated square-pyramidal $[CdCl_5]^{3-}$ anions and triethylbenzylammonium $(C_6H_5CH_2N(C_2H_5)_3)^+$ cations, which are interconnected via $C-H \cdots Cl$ weak hydrogen bonds forming 3D network. Investigation of RT-XRPD was carried out to identify the purity of the bulk material. Hirshfeld surface and fingerprint plots reveal that the structure is dominated by $H \cdots H$ and $H \cdots Cl/Cl \cdots H$ contacts. It is found that the $(C_6H_5CH_2N(C_2H_5)_3)CdCl_3$ material displays a irreversible structural phase transition at $T = 413$ K. This latter was confirmed by means of variable temperature X-ray powder diffraction and dielectric permittivity (ϵ' and ϵ'').

Keywords: Trichlorocadmate hybrid material, Hirshfeld surface analysis, RT-XRPD, Structural phase transition, VT-XRPD, Dielectric properties.

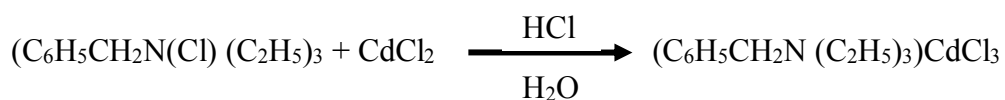
1. Introduction

Many investigations have been focused on the elaboration of new organic-inorganic hybrid compounds with the formula ABX_n have widely studied in recent years (where A = organic molecule, B = transition metal and X= Cl, Br, I). These materials received considerable attention as they possess several applications in various domains and interesting properties such as photoluminescence^[1], optical^[2], excellent magnetic, dielectric^[3] and fluorescent properties^[4]. Moreover, organic halidometallates have received increasing attention because their various phase transition in which some physical properties change around the transition temperature. However, the stability of these materials is essentially ensured by non-covalent intermolecular interactions such as hydrogen bonds between cationic and anionic components, which provide freedom to the molecular motion of the organic cation. Although many types of phase transition have been found, searching for new phase transition compounds drives continuous investigations for new types of organic-inorganic compounds. The organic-inorganic metal halides are excellent candidates to prepare phase transition materials, and we opted for Cd^{2+} because it exhibits a variety of coordination numbers and geometries, resulting to the generation of many structures with various dimensionalities and with various physical properties. Referring to the literature, several related structures have already been reported, such as $RCdCl_3$ ^[5]; $RCdCl_3 \cdot H_2O$ ^[6]; RCd_3Cl_8 ^[7]; $RCdCl_4 \cdot H_2O$ ^[8]; $RCd_{1.5}Cl_5$ ^[9]. Within this context, we focus on the preparation and structural characterization of a new trichlorocadmiate compound with the formula $(C_6H_5CH_2N(C_2H_5)_3)CdCl_3$. Hirshfeld surface analysis is introduced in order to evaluate the interactions within the crystal structure. Thermal analysis (TGA and DSC), VT-XRPD and dielectric measurement were performed in order to investigate the structural phase transition around the transition temperature.

2. Experimental

2.1. Chemical preparation

Crystals of $(C_6H_5CH_2N(C_2H_5)_3)CdCl_3$ were obtained by slow evaporation at room temperature by dissolving benzyltriethylammonium chloride $C_6H_5CH_2N(Cl)(C_2H_5)_3$ in a concentrated Hydrochloric Acid (HCl) solution (37%, $d = 1,19 \text{ g/cm}^3$) and Cadmium Chloride ($CdCl_2$) in the stoichiometric 1 : 1 molar proportions. Then the mixture is stirred for 15 min. After some days colorless and transparent crystals were formed suitable for single X-ray diffraction analysis. Chemical reaction is written as follow:



2.2. Spectroscopic measurements

The infrared spectroscopy measurement was performed between 400 and 4000 cm^{-1} wavenumber range with a sample pressed in pure KBr pellet using a Perkin-Elmer FT-IR spectrophotometer 1000. The Raman spectrum was recorded in the wavenumber range from 50 cm^{-1} to 500 cm^{-1} using a LABHARAM HR 800 triple monochromatic.

2.3. X-ray data collection

A single crystal with a size ($0.31 \times 0.24 \times 0.21 \text{ mm}$) was selected using an optical microscope in order to disclose its crystal analysis. Single crystal XRD intensity data were collected at room temperature (293K) using Bruker APEX II diffractometer equipped with graphite monochromated $\text{MoK}\alpha$ radiation (0.71073 Å). The programs used to solve and refine the structure are SHELXS-2014^[10] and SHELXL-2014^[11] respectively. The cadmium and chloride atoms were placed using Patterson method. The organic atoms were found from Fourier calculations. The crystal structure was refined in monoclinic crystal system with $\text{P2}_1/\text{n}$ space group by full-matrix least square. Crystal data, data collection and structure refinement of $(\text{C}_6\text{H}_5\text{CH}_2\text{N}(\text{C}_2\text{H}_5)_3)\text{CdCl}_3$ crystal are summarized in Table 1. Non-hydrogen atoms (cadmium, chloride, carbon) were refined using anisotropic atomic displacement parameters. Factors of anisotropy thermal agitation for $(\text{C}_6\text{H}_5\text{CH}_2\text{N}(\text{C}_2\text{H}_5)_3)\text{CdCl}_3$ were grouped in Table S2. However, hydrogen atoms linked to phenyl ring were refined isotropically. Atomic coordinates and equivalent thermal factors of agitation U_{eq} (Å^2) and isotropic U_{iso} (Å^2)* were summarized in Table S1. Finally, Mercury^[12] and Diamond^[13] software were used to drawing the structural graphics.

2.4. Hirshfeld surface

The Hirshfeld surface analysis is the powerful technique to identify and visualize the intermolecular long or short contacts in the reported cadmium (II) crystal structure. Hirshfeld surfaces were studied using the normalized contact distance (d_{norm}) and the fingerprint plots which are calculated with the program Crystal Explorer^[14] using the CIF format. The d_{norm} was given by the equation (1):

$$d_{\text{norm}} = \frac{d_i - r_i^{\text{vdw}}}{r_i^{\text{vdw}}} + \frac{d_e - r_e^{\text{vdw}}}{r_e^{\text{vdw}}} \quad (1)$$

The d_{norm} is essentially based on terms of d_e (the distance from the Hirshfeld surface to the nearest atom outside the surface) and d_i (distance from the Hirshfeld surface to the nearest atom inside the surface) and the Van Der Walls (VDW) radii of atom. Graphical plots of the molecular Hirshfeld surfaces mapped with d_{norm} used red–white–blue scheme, where red highlights shorter contacts, white is used for contacts around the VDW separation, and blue is

for longer contacts. Moreover, two further colored properties (shape index and curvedness) based on the local curvature of the surface can be specified^[15].

2.5. Thermal properties

In order to give more information about thermal stability of the crystal structure during heating, we investigated the thermal analysis of our compound. The thermogravimetric analyses (TGA) were carried out at the temperature ranging from 300 to 750 K using an ATG PYRIS 6 instrument with a speed of 5°C/min under a nitrogen atmosphere.

The differential scanning calorimetry (DSC) measurements were studied on heating the sample at the rate of 5°C min⁻¹ under an inert atmosphere (nitrogen gas) in the temperature range from 320 to 480 K using DSC 822 METTLER TOLEDO instrument.

2.6. Variable temperature X-ray powder diffraction (VT-XRPD)

X-ray powder diffraction measurements at variable temperature were carried out in Bragg-Brentano geometry with a CuK α radiation on a Rigaku Smartlab XE diffractometer equipped with an Anton Paar TTK600 and a solid-state 2D detector Hypix 3000. Data were collected in the range of 5°–60° 2 θ (°) heating and cooling the sample from 25°C to 180° at 10 °C/min.

2.7. Dielectric measurements

Powder of the compound pressed into a pellet of about 2.57 mm in thickness and 28.26 mm² diameter. Dielectric constant measurements were studied using TEGAM 3550 ALF automatic bridge monitored by a microcomputer. The frequency-dependent constant was registered from 110 MHz to 40 Hz over the temperature range 300 – 420 K.

3. Results and discussion

3.1. Vibrational studies

Vibrational spectroscopy such as IR-spectroscopy and Raman-scattering have been widely undertaken to identify the functional groups present in the crystal and to gain useful information about the crystal structure. The assignment of all bands detected in the infrared spectrum (Fig.1) of the triethylbenzylammonium cation in the title material is essentially based on the comparison with previous similar compounds^{[16][17]}. The bands observed at 2975, 1480, 1449 and 1391 cm⁻¹ were attributed to stretching and deformation vibrations of aliphatic CH. The band observed at 1360 corresponds to the stretching vibration of C–N. The bands appearing between 1206 and 1081 cm⁻¹ were assigned to the in-plane CH deformation mode. The intense band at 1007 cm⁻¹ was assigned to the deformation vibration of C=C. The bands appearing in 822–750 cm⁻¹ were assigned to the C–H out-of-plane deformation of the

phenyl ring. The strong band at 542 was attributed to the deformation vibration of C–N–C. The deformation vibration of C–C–C was observed at 469 cm⁻¹.

The Raman spectrum (Fig.2) illustrates the vibrations of the trichlorocadmate (CdCl₃⁻) anion. The Cd-Cl asymmetric and symmetric stretching was appeared at 370–259 cm⁻¹. The bands observed at 126–98 cm⁻¹ were associated to the deformation mode of Cl–Cd–Cl. The lattice mode was detected at 64 cm⁻¹. The investigation of IR spectra confirms the presence of organic cation (C₆H₅CH₂N(C₂H₅)₃)⁺, while the study of Raman spectra proves the existence of inorganic anion (CdCl₃)⁻.

3.2. Structure description

The single-crystal X-ray study reveals that the title compound, (C₆H₅CH₂N(C₂H₅)₃)CdCl₃, crystallizes in the centrosymmetric P2₁/n space group of the monoclinic system with four formula units. An ORTEP drawing of the asymmetric unit (Fig.3), illustrates that it is comprised of one trichlorocadmate(II) anion (CdCl₃)⁻ and one triethylbenzylammonium cation (C₆H₅CH₂N(C₂H₅)₃)⁺. The examination of the crystal structure demonstrates that the atomic arrangement consist of 1-D polymeric chains of square-pyramidal CdCl₅ developing in the direction of a-axis. The cationic groups are regulary intercalated between these anionic chains. A perspective view of the crystal packing (Fig.4), shows that the cohesion of the [CdCl₅]_n polymeric chains with the organic cations is ensured through C··H–Cl hybrid bonds resulting of the crystal structure. The geometric parameters of hydrogen bonds are reported in Table 2. A perspective view of the inorganic part (Fig.5), shows that The 1-D polymeric chains of square–pyramidal CdCl₅ are linked to each other via Cl^{II} and Cl^{II} chlorine atoms (i: -x,-y,-z) to form zigzag chains. Each cadmium(II) ion is coordinated by five chlorine atoms, Cl₁, Cl₂, Cl₁ⁱ and Cl₂ⁱ atoms occupied the basal plane while Cl₃ atom takes the apical position. The bond distances of Cd–Cl ranging from 2.446(1)Å to 2.778(3)Å and the bond angles of Cl–Cd–Cl varied between 83.610(15)° and 170.612(13)°. The dihedral angle value between various planes Cl^{II}–Cd–Cl^{II}–Cd and Cd–Cl₂–Cd–Cl₂ is equal to 57.95°. Bond distances and angles for (CdCl₅)⁻ are reported in Table 3. Geometric parameters of (CdCl₃)⁻ anion are comparable to those found in the Cambridge Structural Database (CSD) for other structurally similar chlorocadmate (II) compounds containing CdCl₃, (C₉H₁₄N)CdCl₃^[18], (C₈H₂₀N)CdCl₃^[19], (C₃H₄NS)CdCl₃^[20], (C₅H₁₂N)CdCl₃^[21] and [N(CH₃)₃H]CdCl₃^[22].

Taking into account the geometrical parameters characteristics of the entities, the average values of the Baur distortion indices are calculated by means of equations (2) and (3)^[23]:

$$\text{ID}(\text{Cd} - \text{Cl}) = \sum_{i=1}^{n_1=5} \frac{|d_i - d_m|}{n_1 d_m} \quad (2)$$

$$\text{ID}(\text{Cl} - \text{Cd} - \text{Cl}) = \sum_{i=1}^{n_2=10} \frac{|a_i - a_m|}{n_2 a_m} \quad (3)$$

Where d: (Cd–Cl) distance; a: (Cl–Cd–Cl) angle; m: average values; n_1 and n_2 are equal to 5 and 10 respectively.

We found $\text{ID}(\text{Cd} - \text{Cl}) = 0.00912$ and $\text{ID}(\text{Cl} - \text{Cd} - \text{Cl}) = 0.01908$; these low values of the Baur distortion indices indicate that the coordination of the cadmium metal is slightly distorted square-pyramidal.

The organic part of the title compound is formed by one $(\text{C}_6\text{H}_5\text{CH}_2\text{N}(\text{C}_2\text{H}_5)_3)^+$ cation, with no significant distortions from average bond lengths and angles. Benzene rings of the organic cations do not approach in the packing, showing a centroid–centroid distance of 9.434 Å, excluding stacking interactions.

3.3. Hirshfeld surfaces analysis

Hirshfeld surfaces and 2D fingerprint plots were investigated in order to identify and to explore intermolecular interactions which ensure the cohesion of the crystal packing.

Fig.6 displays Hirshfeld surfaces mapped with d_{norm} , shape index and curvedness depicting intermolecular interactions in the studied compound $(\text{C}_6\text{H}_5\text{CH}_2\text{N}(\text{C}_2\text{H}_5)_3)\text{CdCl}_3$. Hirshfeld surfaces mapped over d_{norm} surface reveals red spots which correspond to C–H \cdots Cl interactions. The nature of contacts (either donor or acceptor) on the Hirshfeld surfaces can easily be identified on a shape index. The surface area over the acceptor is red and over donor is blue on the shape index^[24]. The red spot over carbon indicates that carbon atoms are donors, while the blue spot over chlorine indicates that chlorine atoms are acceptor. Whereas curvedness maps are most suitable for identifying the $\pi \dots \pi$ stacking interactions in the compound.

The 2D fingerprint plots for atom-atom contacts and the percentage contribution of each contact to the Hirshfeld surfaces in $(\text{C}_6\text{H}_5\text{CH}_2\text{N}(\text{C}_2\text{H}_5)_3)\text{CdCl}_3$ are shown in Fig.7. The examination of 2D fingerprint plots discloses that H \cdots H and Cl \cdots H/H \cdots Cl contacts contribute maximum in the cohesion and stabilization of the crystal packing. The contributions of H \cdots H and Cl \cdots H/H \cdots Cl contacts intermolecular interactions to the total surface Hirshfeld are 42.3% and 36.9%, respectively. Other intermolecular contacts such as C \cdots H (9.1%), Cd \cdots Cl (8.7%), Cd \cdots H (1.9%), Cl \cdots Cl (1.1%) contribute less to the total surface Hirshfeld.

3.4. Room temperature X-ray powder diffraction (RT-XRPD)

The X-ray diffraction (XRD) is known as a useful technique for determining the phase purity of solid samples^[25]. Crystals of $(\text{C}_6\text{H}_5\text{CH}_2\text{N}(\text{C}_2\text{H}_5)_3)\text{CdCl}_3$ were finely crushed and were analyzed using X-ray powder diffraction at room temperature. Fig.8 illustrates experimental and calculated powder patterns at different 2θ ranging from 5° to 60° . As shown, the pattern simulated from single X-ray diffraction at room temperature coincides with experimental powder pattern, manifesting a pure phase of the sample.

3.5. Thermal properties

The result of thermogravimetric (TGA) analysis for the $(\text{C}_6\text{H}_5\text{CH}_2\text{N}(\text{C}_2\text{H}_5)_3)\text{CdCl}_3$ material is illustrated in Fig.9. TGA curve shows that the compound possesses a considerable thermic stability (up to $T = 520$ K), no weight loss was observed in the temperature range 300–520 K. This stability is due to the cumulative effect of the various weak interactions ($\text{C}-\text{H}\cdots\text{Cl}$). Beyond $T = 520$ K, the compound occurs one weight loss (calculated weigh loss= 38.82%, theoretical weigh loss = 55.3%), which is more probably corresponds to the partial decomposition of the organic benzyltriethylammonium chloride moiety.

DSC thermogram (Fig.10) shows that the compound occurred one anomaly thermic at around $T = 413$ K during the heating. This intense endothermic peak corresponds to a first order phase transition^[26]. During the cooling, no feature is observed indicating that this transition is not reversible. The enthalpy and entropy value of the phase transition are $\Delta H = 62.012$ J/g and $\Delta S = 0.15$ J/g.K, respectively. The ΔS is related to the number of orientations in the two phases by Boltzmann's equation (4):
$$\Delta S = R * Ln \left(\frac{n_2}{n_1} \right) \quad (4)$$

Where n_1 and n_2 are the number of orientations in the higher and lower temperature phases respectively and R is the Universal gas constant ($8.31 \text{ J}\cdot\text{mol}^{-1}\cdot\text{K}^{-1}$). n_2/n_1 ratio values for order-disorder processes generally from 1.3 and 48. In our case $n_2/n_1 = 1.118$, indicating that the phase transition detected at $T = 413$ K is not an order-disorder type. More probably the phase transition can be classified structural.

3.6. Variable temperature X-ray powder diffraction (VT-XRPD) analysis

Investigation of VT-XRPD is essentially undertaken to understand the solid-state changes during heating and to identify phase transition. Fig.11 reveals the successive powder patterns obtained by heating the trichlorocadmate hybrid compound from 25°C to 180°C . In the temperature range $25^\circ\text{C} - 135^\circ\text{C}$, all the powder patterns did not change and seems to be

similar during heating, indicating the stability of the crystal structure (phase I). Above these temperatures, some original peaks disappear and the intensities of the main reflections in the powder patterns change. The intensity of the highest reflection peak at $2\theta = 8.3^\circ$ decreases abruptly, which indicates that new phase (phase II) formed. This result indicates that the phase transition is accompanied with rearrangement of the structure during the transition temperature ($T = 140^\circ\text{C}$); which is in good correlation with the DSC analysis.

To ensure phase transition reversibility, an X-ray powder diffraction cooling cycle was studied in the temperature range $151 - 25^\circ\text{C}$ (Fig.12). From this result, it is clearly observed that the title material ($\text{C}_6\text{H}_5\text{CH}_2\text{N}(\text{C}_2\text{H}_5)_3\text{CdCl}_3$) exhibits irreversible phase transition. Furthermore, these results were in agreement with DSC analysis.

3.7. Dielectric constant analysis

The complex permittivity formalism has been employed to give useful information about the chemical and physical behavior of the electrical and dielectric properties. The expression (5) of the dielectric constant is written as follow ^[27]:

$$\varepsilon^*(\omega) = \varepsilon' - j\varepsilon'' \quad (5)$$

Where ε' and ε'' are the real and imaginary parts of the complex permittivity, respectively.

The temperature dependences of the real (ε') and imaginary (ε'') parts of the dielectric permittivity for the studied compound ($\text{C}_6\text{H}_5\text{CH}_2\text{N}(\text{C}_2\text{H}_5)_3\text{CdCl}_3$) at different frequencies are shown in Fig.13. At low temperature (up to 400 K), the variations of the dielectric constants (ε' and ε'') with temperature are almost constants. This phenomenon may be explained by the restricted reorientational motions of the cation moiety which cannot orient themselves and cannot flow the direction of applied electric field ^[28]. Beyond $T = 400$ K, the variation of ε' and ε'' parts start to increase sharply with increasing of temperature and its value strongly depends on the frequency, which could be related to the increase of disorder in the material. This disorder induced weakens forces of hydrogen bonds and electrostatic interaction. However, charge carriers can orient themselves with respect to the direction of applied electric field. This behavior could be due to the accumulation several mechanisms, such as that the reorientational dynamics of organic groups is activated and the increase of the mobility of charge carriers^[27]. At high temperature the compound undergoes a dielectric anomaly (up to $T = 420$ K) associated with the structural phase transition detected by DSC measurements.

Conclusion

In summary, a new organic-inorganic hybrid compound, $(\text{C}_6\text{H}_5\text{CH}_2\text{N}(\text{C}_2\text{H}_5)_3)\text{CdCl}_3$, has been synthesized at room temperature by slow evaporation. The results of single X-ray diffraction illustrate that the studied compound belongs to the monoclinic system with the $\text{P2}_1/\text{n}$ space group. The atomic arrangement of the crystal structure can be described as 1D polymeric anionic chain CdCl_3 developing in the direction of a-axis, between which organic cations are intercalated. The cohesion of the crystal packing is essentially ensured by coulombic cation...anion interactions combined with intermolecular $\text{C}-\text{H}\cdots\text{Cl}$ weak hydrogen bonds, forming 3D supramolecular network. Vibrational spectroscopies (IR and Raman) prove the presence of both organic $(\text{C}_6\text{H}_5\text{CH}_2\text{N}(\text{C}_2\text{H}_5)_3)^+$ and inorganic $(\text{CdCl}_3)^-$ parts. Investigation of intermolecular interactions and crystal lattice via Hirshfeld surface analysis demonstrates that $\text{H}\cdots\text{H}$ (42.3%) and $\text{Cl}\cdots\text{H}/\text{H}\cdots\text{Cl}$ (36.9%) contacts intermolecular interactions are the most dominant in the stabilization of the crystal structure. Powder X-ray diffraction at room temperature confirms the phase purity of the bulk material. TGA thermogram reveals that the material is stable until $T = 520$ K. Thermal analysis (DSC) discloses that the compound undergoes an irreversible structural phase transition at the temperature around $T = 413$ K. The results obtained from VT-XRPD analysis and thermal analyses (TGA and DSC) were found to be in good correlation with each other. The real and the imaginary parts of the dielectric constant, decrease as the frequency increase and increase as the temperature increase.

Supplementary Material

Crystal data for a new centrosymmetric compound $(C_6H_5CH_2N(C_2H_5)_3)CdCl_3$, has been deposited at the Cambridge Crystallographic Data Center as supplementary publications **CCDC 1875498**. Data can be obtained free from charge from the Cambridge Crystallographic Data Center, 12 Union Road, Cambridge CB2 1EZ, UK, Fax: +441223336033; E-mail: deposit@ccda.cam.ac.uk.

Acknowledgements

The authors would like to thank all members of the unit of common services at the University of Sfax. The authors would like to convey special thanks to the members of unit at the University of Parma for their assistance in the measurements for single X- ray diffraction and X-ray powder diffraction. This work has benefited from the equipment and framework of the COMP-HUB Initiative at the University of Parma, funded by the ‘Departments of Excellence’ program of the Italian Ministry for Education, University and Research (MIUR, 2018-2022). The authors are also grateful to Pro Kamel Khirouni for their support concerning the dielectric measurements.

References

- [1] M. S. Lassoued, A. Lassoued, M.C.M. Abdelbaky, S.Ammar, A.Gadri, A.Ben Salah, S.Garcia-Granda, *J. Mol. Struct.*(2017), vol. 1141, pp. 660–667.
- [2] M. Hajji, A. Gharbi, T. Guerfel, *J. Inorg. Organomet. Polym.*(2014), vol. 24, pp. 766-775.
- [3] M. S. Lassoued, A. Lassoued, M. S. M. Abdelbaky, S. Ammar, A. Gadri, A. Ben Salah, S. Garcia-Granda, *J. Mater. Sci* (2018), vol. 29, pp.5413–5426.
- [4] M. Guerrero, J. Pons, J. Ros, M. Font-Bardia, O. Vallcorba, J. Rius, V. Branchadell, A. Merkoci, *J.Cryst. Eng. Comm* (2011), vol. 13, pp. 6457–6470.
- [5] Y. Lu, Z. Wang, H-P. Chen, J-Z. Ge, *J. Cryst Eng Comm* (2017), vol. 5, pp. 1-3.
- [6] S. Soudani, E. Jeanneau, C. Jelsch, F. Lefebvre, C. Ben Nasr, *J. Solid State Sci* (2016), vol. 57, pp. 49–55, 2016.
- [7] N. Karâa , B. Hamdi, A. Ben Salah, *J. Mol. Struct* (2012), vol. 1013, pp. 168–176.
- [8] M. S. Lassoued, W. Ben, S. Mohammed, S. Ammar, A. Gadri, A. Ben. Salah, S.Garcia-Granda, *J. Mater. Sci. Mater. Electron.*(2017), vol. 28, pp. 12698–12710.
- [9] M. Hajji, C. Kouraichi, T. Guerfel, *J.Bull. Mater. Sci* (2017), vol. 40, pp. 55–66.
- [10] G. M. Sheldrick, “A short history of SHELX”(2008), pp. 112–122.
- [11] G. M. Sheldrick, “Crystal structure refinement with SHELXL”(2014), pp. 3–8.
- [12] C.F.Macrae, P.R.Edgington, P.MacCabe, E.Pidcock, G.P.Shields, R.Taylor, M.Towler, J.van de Streek, *J.Appl. Cryst.* (2006), vol. 39, pp. 453–457.
- [13] P. Humezra, G. K. , Zerrin Heren, Kamber Akdag, *Acta Cryst.* (2009), vol. 65, pp. 279.
- [14] J. J. Mckinnon, A. Mark, S. Anthony, *Acta. Cryst.* (2004), vol. 60, pp. 627-668.
- [15] Jan J Koenderink, Andrea J van Doorn, *Image Vis. Comput.* (1992), vol. 10, no. 8, pp. 557–564.
- [16] [18] W. Amamou, H. Feki, N. Chniba-Boudjada, F. Zouari, *J. Mol. Struct.*(2014), vol. 1059, pp. 169–175.
- [17] I. Chaabane, F. Hlel, and K. Guidara, *J. PMC Phys. B* (2008), vol. 1, pp. 11.
- [19] S. Lakshmi, M. A. Sridhar, J. Shashidhara Prasad, G. Amirthaganesan, M. A. Kandhaswamy, V. Srinivasan, *J. Anal. Sci.*(2004), vol. 20, pp. 57–58.

- [20] G. Mei, W. Liao, *J. Mater. Chem. C.* (2015), vol. 3, pp. 8535–8541.
- [21] Y. Zhang, H. Ye, W. Zhang, R. Xiong, *J. Inorg. Chem. Front.*(2014), vol.1, pp. 118–123.
- [22] H. Kchaou, K. Karoui, A. Ben Rhaïem, *J. Physica E* (2017), vol. 85, pp. 308–315.
- [23] M. Hughes, F. Foit, and E. Wright, *J. Polyhedron* (2002) vol. 40, pp. 153–162.
- [24] Bhavesh N. Socha, Urmila H. Patel, Sachin B. Pandya, Bhavin R.Chayda, Kaushik P. Chaudhary, Bharatkumar D. Patel, R.H.Patet, Nikita J. Patel, Bhupesh S. Bhatt, *J. Polyhedron* (2020).
- [25] H. Aghaei, M. Ghavi, G. Hashemkhani, M. Keshavarz, *J. Biol. Macromol.* (2020), vol 162, pp. 74–83.
- [26] Mark Hindmarsh, Stephan J. Huber, Kari Rummukainen, David J. Weir, *J. Phys. Rev. Lett.* (2014), vol. 41301, pp. 1–5.
- [27] H. E. Sekrafi, A. B. J. Kharrat, M. A. Wederni, K. Khirouni, N. Chniba-Boudjada, W. Boujelben, *J. Mater. Res. Bull.* (2018), vol.111, pp.329-337.
- [28] R. Hajji, A. Oueslati, N. Errien, F. Hlel, *J. Polyhedron* (2014), vol.79, pp.97-103.
- [29] N. Chihaoui, B. Hamdi, R. Zouari, *J. Mol. Struct.*(2017), vol. 1147, pp.48-55.